

NON-UNIVERSALITY OF DARK-MATTER HALOS: CUSPS, CORES, AND THE CENTRAL POTENTIAL

JENS HJORTH¹, LILIYA L. R. WILLIAMS², RADOSŁAW WOJTAK^{1,3}, AND MICHAEL McLAUGHLIN²

Received 2014 February 17; accepted 2015 August 8

ABSTRACT

Dark-matter halos grown in cosmological simulations appear to have central NFW-like density cusps with mean values of $d \log \rho / d \log r \approx -1$, and some dispersion, which is generally parametrized by the varying index α in the Einasto density profile fitting function. Non-universality in profile shapes is also seen in observed galaxy clusters and possibly dwarf galaxies. Here we show that non-universality, at any given mass scale, is an intrinsic property of DARKexp, a theoretically derived model for collisionless self-gravitating systems. We demonstrate that DARKexp—which has only one shape parameter, ϕ_0 —fits the dispersion in profile shapes of massive simulated halos as well as observed clusters very well. DARKexp also allows for cored dark-matter profiles, such as those found for dwarf spheroidal galaxies. We provide approximate analytical relations between DARKexp ϕ_0 , Einasto α , or the central logarithmic slope in the Dehnen–Tremaine analytical γ -models. The range in halo parameters reflects a substantial variation in the binding energies per unit mass of dark-matter halos.

Subject headings: dark matter — galaxies: halos — galaxies: kinematics and dynamics

1. INTRODUCTION

The basic shape of N-body simulated cold dark matter halos is now well established. The NFW density profile (Navarro et al. 1997) is a remarkably good representation (e.g., Tasitsiomi et al. 2004; Diemand et al. 2004, 2005a,b; Navarro et al. 2010; Diemand & Moore 2011; Ludlow et al. 2011), especially given its simplicity: it has no shape parameters. However, a closer examination of the profile shapes of relaxed halos shows that NFW does not fully capture the density run. Most importantly, while the NFW profile has a central density cusp, with logarithmic slope $d \log \rho(r) / d \log r = -1$, recent high resolution simulations have shown that the central cusp tends to become somewhat shallower at smaller and smaller radii (e.g., Navarro et al. 2010), prompting the use of an Einasto α -model (Navarro et al. 2004; Einasto 1965). The Einasto profile fits halos better at most radii, not just in the center, suggesting that the additional parameter α is a real characteristic of dark matter halos (Merritt et al. 2006; Klypin et al. 2014).

Ludlow et al. (2013) find that the mean value of α ranges from about 0.17 for $M_{200} = 10^{11} h^{-1} M_{\odot}$ halos to 0.21 at $M_{200} = 10^{15} h^{-1} M_{\odot}$, which is consistent with Gao et al. (2008) who find a relation between Einasto’s α and the ratio of the linear density threshold for collapse to the rms linear density fluctuation at a given mass scale. In addition to the mass-dependent α , there is significant scatter of around 0.05 in α . Moreover, halos with α in the range 0.05 to 0.45 are also realized in simulations (Ludlow et al. 2013; Klypin et al. 2014). These works show that the shape of the density profile, including the central logarithmic slope, is tied to the ini-

tial conditions and evolutionary history of the halos in simulations. Ludlow et al. (2013) suggest that the mass profiles of halos reflect their accretion history.

The spread in α index is observed not just for main halos, but also subhalos. Springel et al. (2008) find that the profiles of subhalos do not converge to a central power law but exhibit curving shapes well described by the Einasto form with α in the range 0.15 to 0.28. This is consistent with the findings of Vera-Ciro et al. (2013), who note that simulated satellite dark matter halos around galaxies are better fit with Einasto profiles of index $\alpha = 0.2 - 0.5$. Di Cintio et al. (2013) find a correlation between α^{-1} (ranging from 0.1 to 1) and satellite dark matter halo mass, i.e., with higher masses corresponding to smaller values of α , contrary to the trend found for more massive halos. The diversity in the density profiles of these satellites is attributed to tidal stripping, which acts mainly in the outer parts of the subhaloes.

The conclusion is that simulated dark matter halos do not form a strictly self-similar family of systems as was originally suggested, but display non-universality (Merritt et al. 2006).

Neither NFW nor Einasto have any theoretical underpinnings; they are purely empirical. In a series of papers (Hjorth & Williams 2010; Williams & Hjorth 2010; Williams et al. 2010, 2014) we have proposed a theoretically based model, DARKexp, which has been shown to allow good fits to a few simulated halos (Williams et al. 2010, 2014) and observed galaxy clusters (Beraldo e Silva et al. 2013; Umetsu et al. 2015).

DARKexp has one shape parameter, and its density profiles are very similar to Einasto within a limited range of shape parameters. Taking the broader range of achievable values into account, DARKexp suggests that there should be a dispersion in the shapes of the density profiles between systems, parametrized by the shape parameter. At small radii, but sufficiently above the resolution limit achieved in cosmological simulations, these density profiles differ significantly. Some have nearly flat cores, while

¹ Dark Cosmology Centre, Niels Bohr Institute, University of Copenhagen, Juliane Maries Vej 30, DK-2100 Copenhagen Ø, Denmark; jens@dark-cosmology.dk

² School of Physics and Astronomy, University of Minnesota, 116 Church Street SE, Minneapolis, MN 55455, USA; llrw@astro.umn.edu

³ Kavli Institute for Particle Astrophysics and Cosmology, Stanford University, SLAC National Accelerator Laboratory, Menlo Park, CA 94025, USA

others are steep, $d \log \rho(r)/d \log r \approx -2$. In other words, unless halos have identical normalized central potentials, DARKexp predicts that the density profiles should not be universal, and that a logarithmic slope of -1 at small radii robustly resolved in simulations is not a universal attractor of halos with different formation histories. Testing this would be important because DARKexp is not a fitting function but is derived from basic physics.

We summarize the rationale and properties of DARKexp in Section 2. While DARKexp has the advantage of being derived from first principles, the resulting density profiles unfortunately cannot be expressed analytically. We therefore also relate the properties of DARKexp to those of phenomenological fitting functions, i.e., generalized Hernquist, Dehnen–Tremaine, and Einasto models. We discuss non-universality of simulated and observed massive dark-matter halos in Section 3 and show that, in cases where exact fits are not required, DARKexp, Einasto, or Dehnen–Tremaine profiles provide equally good representations, with considerable dispersion in their respective shape parameters. We relate observed, simulated and theoretical properties of lower mass halos in Section 4 and conclude in Section 5

2. DARKEXP AND THE CENTRAL POTENTIAL–DENSITY SLOPE RELATION

DARKexp is a theoretical model for the differential energy distribution in a self-gravitating collisionless system. Specifically, defining $N(\epsilon) = dM/d\epsilon$, where ϵ is the normalized absolute particle energy per unit mass, a statistical mechanical analysis leads to

$$N(\epsilon) \propto \exp(\phi_0 - \epsilon) - 1 \quad (1)$$

(Hjorth & Williams 2010). The central dimensionless potential, ϕ_0 , is the only free shape parameter of the model. Some of the global properties of the model are analytic (see Appendix A), while the phase space distribution function and derived properties, such as the density profile, must be obtained numerically using an iterative procedure (Williams et al. 2010). Apart from the assumption of isotropy (which leads to spherical structures), there are no additional assumptions involved in this computation. The scale parameters of the corresponding density profile follow from the resulting profiles themselves. DARKexp is a maximum entropy theory and as such describes only the final, equilibrium states of systems, and not the evolutionary paths that brought them to the final state. The density profiles apply to isolated systems, i.e., there is no cosmological context and so no concept of a virial radius or formation redshift.

While the asymptotic logarithmic density slope is -1 for $r \rightarrow 0$ (Hjorth & Williams 2010), in reality the central logarithmic slope robustly resolved in simulations depends on ϕ_0 : $\phi_0 \lesssim 4$ systems have inner logarithmic slopes shallower than -1 , while $\phi_0 \gtrsim 5$ have inner logarithmic slopes between -1 and -2 (Williams & Hjorth 2010). DARKexp was not designed to fit the properties of dark-matter structures. Nevertheless, the energy distributions resulting from this first principles derivation are excellent representations of numerical simulations and the density profiles are reminiscent of Einasto α profiles for values of ϕ_0 around 4 (Williams et al. 2010). Note that in the Williams et al.

(2014) formalism, the DARKexp density run is independent of any velocity anisotropy. DARKexp also provides very good fits to observed galaxy clusters (Beraldo e Silva et al. 2013; Umetsu et al. 2015), and globular clusters (Williams et al. 2012).

We here compare DARKexp to phenomenological fitting functions, notably the generalized Hernquist, the special case of the Dehnen–Tremaine γ -model, and the Einasto profile (see Appendix B for details).⁴ We provide the correspondence between the shape parameters of these analytic fitting functions and the dimensionless parameter of DARKexp, ϕ_0 . These results can be used in any situation where fitting with DARKexp is required.

By construction, the DARKexp energy distribution is discontinuous at the escape energy, and as a consequence the density falls off as r^{-4} at large radii (Jaffe 1987; Hjorth & Madsen 1991). When searching for phenomenological or analytical profiles that may be useful approximations to DARKexp, we recall that the generalized Hernquist (1990) model has the same outer logarithmic slope of -4 as DARKexp, and also allows for a range of central logarithmic slopes,

$$\rho \propto r^{-\gamma}(1+r^\beta)^{(\gamma-4)/\beta}, \quad (2)$$

where β governs the sharpness of the transition between the asymptotic inner logarithmic slope of $-\gamma$ and the outer logarithmic slope of -4 . For $\beta = 1$ the resulting γ -models,

$$\rho \propto r^{-\gamma}(1+r)^{\gamma-4}, \quad (3)$$

are largely analytical (Dehnen 1993; Tremaine et al. 1994).

Another phenomenological model, which provides an excellent fit to numerical simulations, is the Einasto model (Navarro et al. 2004); it is controlled by the shape parameter α ,

$$\rho \propto \exp\left[-\frac{2}{\alpha}(r^\alpha - 1)\right]. \quad (4)$$

As shown by Williams & Hjorth (2010) and Williams et al. (2010), DARKexp halos have a range of logarithmic slopes at small radii robustly resolved in simulations depending on ϕ_0 ; models in a range around $\phi_0 \approx 4$ are well represented by Einasto models with α in the range 0.15–0.2.

To investigate the relations between the shape parameters describing DARKexp and phenomenological models we now turn to a detailed comparison of their density profiles (see Appendix B). For DARKexp of a given ϕ_0 we find an Einasto model or γ -model that matches DARKexp (i.e., has the same value as DARKexp) in either density or log–log slope. The anchor radius at which the matching is done is chosen to be $\log(r_a/r_{-2}) = -1.5$, which is the typical resolution limit in cosmological simulations (e.g., Navarro et al. 2010). We choose to anchor the profiles at a fixed radius rather than fitting the (log) density or slope as a function of (log) radius, over some range, for visual clarity.

Figure 1 summarizes the results of the matching between DARKexp and phenomenological models. It shows

⁴ For convenience we are making numerically generated models for $\phi_0 = 1$ –10 available for download at the DARKexp website <http://www.dark-cosmology.dk/DARKexp/>.

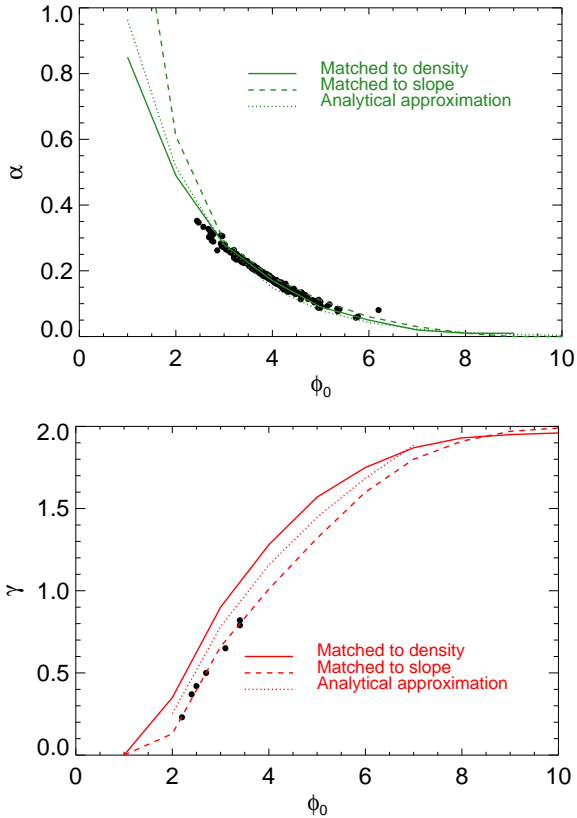


Figure 1. ϕ_0 - α relation (top) and ϕ_0 - γ relation (bottom) for DARKexp. The solid curves are for match in density, the dashed curve are for match in logarithmic slope at $\log(r_a/r_{-2}) = -1.5$. The dotted curves represent analytical approximation to these relations (Equations 5 and 6). In the top panel, the black symbols represent simulated halos (Section 3.1, Figure 3). In the bottom panel, the black symbols are clusters of galaxies from Newman et al. (2013a), obtained as discussed in the text (Section 3.2).

the relations between ϕ_0 and either γ or α , matched in either density or logarithmic slope. We also provide analytical approximations to these relations. For the γ -model

$$\gamma \approx 3 \log \phi_0 - 0.65; \quad 1.7 \leq \phi_0 \leq 6, \quad (5)$$

which suggests $\phi_0 \approx 3.5$ for $\gamma = 1$. For the Einasto model

$$\alpha \approx 1.8 \exp(-\phi_0/1.6) \quad (6)$$

and $\phi_0 \approx 3.8$ for $\alpha = 0.17$.

Comparisons between DARKexp and the empirical models, using the above analytical relations, are shown in Figure 2. We will return to the central potential-density slope relation in the following sections.

3. NON-UNIVERSALITY OF MASSIVE HALOS

3.1. Simulated dark matter halos

Until about 5–10 years ago simulation results were consistent with halos being universal in shape. Now, there is considerable evidence to the contrary. How does the DARKexp expectation of non-universality compare to simulations? We here analyze recent simulations, show that DARKexp fits the density profiles at least as well as Einasto, and quantify the non-universality.

We use cluster halos identified in the Bolshoi simula-

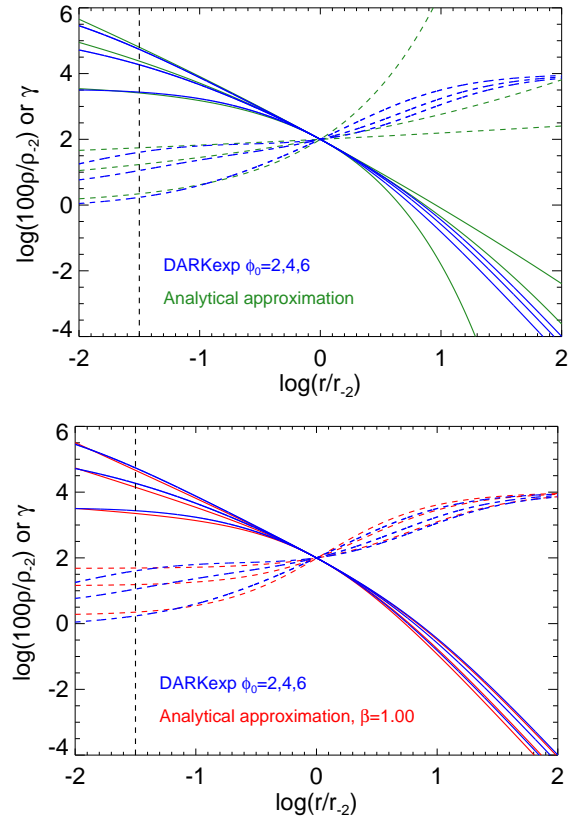


Figure 2. Comparison of DARKexp with Einasto (top) and γ -models (bottom), using the analytical ϕ_0 - α relation (Equation 6, top panel) or the analytical ϕ_0 - γ relation (Equation 5, bottom panel). DARKexp models with $\phi_0 = 2, 4, 6$ (from bottom to top at small radii) are shown in blue (solid curves: density profile; dashed curves: logarithmic density slope).

tion⁵, a dark matter-only simulation run in a $250h^{-1}\text{Mpc}$ box (WMAP5 cosmological parameters) with 2048^3 particles, which corresponds to a mass resolution of $1.35 \times 10^8 h^{-1}M_\odot$ (for more details, see Klypin et al. 2011). For the purpose of our analysis, we select well-resolved equilibrium halos with at least 5×10^5 particles within the virial radius r_v (defined as the radius of a sphere, whose enclosed density is 360 times larger than the background density). The state of equilibrium is assessed using two diagnostics: the virial ratio and the relative offset between the minimum of the potential and the halo mass center. We find 261 equilibrium halos defined by the virial ratio less than 1.3 and the mass center offset less than $0.05r_v$, which are two commonly used relaxation criteria proposed by Neto et al. (2007). This selection is done in order to make a meaningful comparison with DARKexp, which by definition only applies to equilibrium systems.

We calculate the density profiles in 30 spherical shells equally spaced in a logarithmic scale of radius spanning the range from r_{\min} to r_v , where $r_{\min} = 0.015r_v$ is the convergence radius defined by Power et al. (2003) and estimated for the minimum number of particles per halo. The halo centers are given by the minimum of the poten-

⁵ The simulation is publicly available through the MultiDark database (<http://www.multidark.org>). See Riebe et al. (2013) for details of the database.

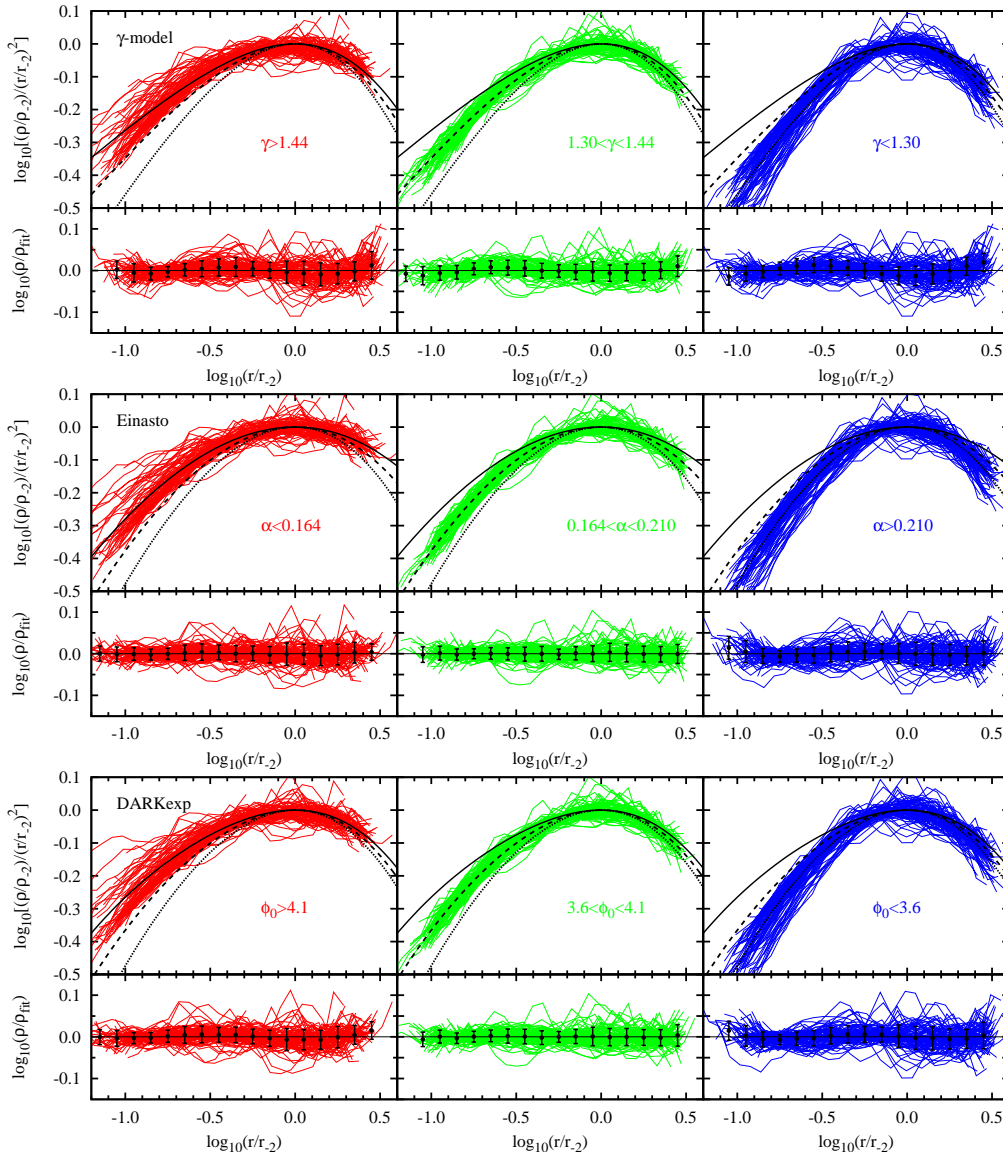


Figure 3. Spherically averaged density profiles of cluster-sized equilibrium dark matter halos formed in cosmological simulations. The profiles are split into three subsamples (columns) corresponding to three ranges of the best-fit shape parameter α of the γ profile (top), Einasto profile (middle) or the best-fit central potential ϕ_0 of DARKexp (bottom). The black curves are the γ (top), Einasto (middle), or DARKexp (bottom) profiles for the mean γ , α or ϕ_0 in the corresponding halo sample (solid curves: $\gamma > 1.44$, $\alpha < 0.164$, $\phi_0 > 4.1$; dashed curves: $1.30 < \gamma < 1.44$, $0.164 < \alpha < 0.210$, $3.6 < \phi_0 < 4.1$; dotted curves: $\gamma < 1.30$, $\alpha < 0.210$, $\phi_0 < 3.6$). The lower panels in either row show the residuals from the best fitting profiles. DARKexp provides as good fits to the simulated halos as the Einasto profile and accounts for the range in properties revealed here.

tial. DARKexp, Einasto, and Dehnen–Tremaine models are fitted to the density profiles of the halos by minimizing the following function

$$\chi = \sum_{i=1}^{n_{\text{shell}}} [\ln \rho_i - \ln \rho_{\text{model}}(r_i)]^2, \quad (7)$$

where n_{shell} is the number of shells and r_i is the mean radius of particles inside the i -th shell. Following Ludlow et al. (2011), we restrict all fits to the radial range $r_{\text{min}} < r < 3r_{-2}$, which prevents including dynamically less relaxed parts of the halos. Here, r_{-2} is defined as the radius at which $d \log \rho(r) / d \log r = -2$, and $\rho_{-2} = \rho(r_{-2})$. We first estimate r_{-2} by fitting an Einasto profile in all 30 shells, i.e., within the radial range

$r_{\text{min}} < r < r_{\text{v}}$. This sets the restricted fitting range to be the same in both cases. Next, r_{-2} , ρ_{-2} , and γ , α or ϕ_0 are obtained from a restricted fit to either model. In fitting DARKexp, we used density profiles computed on a grid of ϕ_0 , ranging from 2.0 to 8.0 with an interval of 0.01.

Figure 3 shows the density profiles of all halos selected for the analysis, in three ranges of the shape parameter, i.e., α for the Einasto model, γ for the Dehnen–Tremaine model, and ϕ_0 for DARKexp. The ranges were chosen such that there are equal numbers of halos in each of the three bins. The mean value of γ is 1.36 with an rms scatter of 0.18 while the mean value of α is 0.19 (rms scatter 0.05). For ϕ_0 the mean value is 3.9 (rms scatter 0.6). There is no significant correlation in these pa-

rameters with the mass over the narrow range of masses considered ($10^{14} - 10^{14.8} M_{\odot}$). The lack of any difference between residuals from the best-fitting Einasto, Dehnen–Tremaine, and DARKexp profile leads to the conclusion that *these models recover spherically averaged density profiles of simulated cosmological halos equally well*.

The second important conclusion is that, in the narrow mass range considered, *there is a range of density profile shapes among simulated systems, and that the DARKexp family of models captures that spread very well*. Figure 1 (top) illustrates this pictorially; it shows the best-fit shape parameters of the Einasto and DARKexp fits to the simulated halos; ϕ_0 and α range between 2.5–6 and 0.05–0.35, respectively (γ ranges from 0.8 to 1.7). The scatter in α is about 0.05. As expected (Section 2), the data show a tight relation between the central potential ϕ_0 and the shape parameter α of the Einasto profile, which traces the α – ϕ_0 relations obtained from matching Einasto and DARKexp density profiles.

3.2. Observed clusters of galaxies

Limousin et al. (2008) have emphasized the wide range of central logarithmic slopes inferred observationally for different clusters of galaxies. DARKexp applies to equilibrium collisionless systems, so in addition to dark matter halos it can also be applied to galaxies and clusters that host baryons, regardless of the physical processes that led to the formation of the final equilibrium systems, provided that the evolution and the present state of these systems are not dominated by two-body encounters, and the systems are not far from being spherical. We here show that relaxed galaxy clusters exhibit non-universality that can be described by the DARKexp model.

Newman et al. (2013a) constructed spherically averaged density profiles of seven massive relaxed clusters, using central galaxy kinematics on the smallest scales, strong lensing on intermediate scales and weak lensing on large scales. To separate out dark matter density profiles they subtracted the stellar contribution of the central galaxy assuming constant mass-to-light ratio for the stellar population. The remaining dark matter profiles were fit with cored NFW and generalized NFW (gNFW) forms.

The γ -model we use here and the gNFW differ in the asymptotic outer logarithmic slope (-4 vs. -3), so the differences are confined mostly to radii outside r_{-2} . At $r \lesssim r_{-2}$ the two models are parametrized similarly, therefore one can compare the two models, if one leaves out the outermost radii. The Newman et al. (2013a) cluster profiles extend about 2 decades in radius interior to r_{-2} , and about 0.75 of a decade exterior to r_{-2} , so the bulk of the radial range is usable in the comparison.

We took the Newman et al. (2013a) inner logarithmic slope for each cluster and set it equal to γ . This supplies the vertical axis coordinate in Figure 1 (bottom). We then fit DARKexp directly to Newman et al. (2013a) gNFW fits, excluding the outer radii beyond which the logarithmic slope is steeper than -2.7 (the fits are insensitive to the truncation logarithmic slope for values between -2 and -2.8). This gave us ϕ_0 , plotted along the horizontal axis. The seven galaxy clusters are plotted as solid points in Figure 1 (bottom). They fit well the ϕ_0 – γ relation matched in slope and are consistent with

our proposed analytical approximation (the dotted red line).

From Figure 1 we conclude that clusters are fit with a range of ϕ_0 's, suggesting non-universality. Observed relaxed clusters of galaxies appear to follow DARKexp; and seem to prefer ϕ_0 values about 2–3.5, on average smaller than cluster-sized dark matter halos in pure dark matter simulations, which are fitted with values of ϕ_0 in the range 2–6.

4. DWARF GALAXIES

So far we discussed dispersion in density profiles among massive pure dark matter halos. We next consider the differences between pure dark matter halos and observed low mass systems.

The central density profiles of observed galaxy clusters appear to be, on average, shallower than those of clusters in pure dark matter simulations. Likewise, the central logarithmic slopes of observed dwarf galaxies are shallower than simulated dark-matter subhalos. In this section we discuss the relative energies between the steeper pure dark matter and shallower observed structures. We will show that the differences amount to a large fraction of the total binding energies of the haloes, demonstrating that the differences in central logarithmic slopes or ϕ_0 represent significant differences between the halos in terms of global energetics. Moreover, assuming the difference between two states or halos is brought about by some dynamical or baryonic process, we compute what it would take to induce a transformation between the two, such as the cusp–core transition. Calculating relative (fractional) energetics allows us to bypass the uncertainties and unknowns associated with the specific physical processes that would bring about the transformation.

4.1. Lack of cusps in dwarf galaxies

The differences between the NFW and Einasto descriptions of pure dark matter halos are small in comparison to the differences between dark matter profiles of subhalos/satellite halos and observed dwarf galaxies which may have central cores. Most dwarf galaxies appear to exhibit significant central density cores (Flores & Primack 1994; Moore 1994; Strigari et al. 2006; Gilmore et al. 2007; Walker et al. 2009; Boylan-Kolchin et al. 2011; Walker & Peñarrubia 2011; Amorisco & Evans 2012; Amorisco et al. 2013; Jardel & Gebhardt 2013; Collins et al. 2014). Whether all dwarfs have a universal profile or not is still unclear because of the large uncertainties associated with the measurement of the central logarithmic density slopes (e.g., Strigari et al. 2014); conclusions seem to depend on the sample and the methods used. For example, Adams et al. (2014) claim that dwarfs are consistent with having a universal central logarithmic density slope of -0.63 , with a scatter of 0.28, while Jardel & Gebhardt (2013) claim that individual dwarf spheroidals show considerable scatter around an average logarithmic slope of -1 .

For reviews of this small scale controversy, see Weinberg et al. (2013) and Pontzen & Governato (2014). The suggested solutions to this set of problems are either baryonic or particle in nature. Warm dark matter does not seem to be the solution: Macciò et al.

(2012, 2013) and Shao et al. (2013) find that warm dark matter leads to cusps just like cold dark matter does, although with very small central cores which however are astrophysically uninteresting and much smaller than what is claimed to be present in dwarf satellites. Indeed, Lovell et al. (2014) conclude that warm dark matter halos and subhalos have cuspy density distributions that are well described by NFW or Einasto profiles (see also Lovell et al. 2012). Pontzen & Governato (2012) and Shen et al. (2014) argue that baryonic physics (Governato et al. 2012), via a process similar to violent relaxation, can lead to changes in the potential, specifically, a more shallow potential and hence a core (see also Brook et al. 2012; Zolotov et al. 2012). Alternatively, self-interacting dark matter can produce large cores (Vogelsberger et al. 2012; Rocha et al. 2013; Zavala et al. 2013; Vogelsberger et al. 2014).

4.2. Cusp-core transition

Real systems like dwarf spheroidals may have shallower central logarithmic slopes and larger central regions of near constant density than pure dark matter halos. How does one make the central potential less deep than found in numerical simulations? The change is likely brought about by baryonic physics (Navarro et al. 1996; Governato et al. 2012; Oñorbe et al. 2015) which may induce a transformation from a typical -1 logarithmic slope to a cored halo (Peñarrubia et al. 2012). In our picture this would correspond to a change in the central potential, through some energy injection process. For DARKexp to be valid, this energy injection would have to be collisionless to preserve the assumptions behind the DARKexp derivation. It is interesting to note that the baryonic feedback process proposed by Pontzen & Governato (2012) is not only collisionless but also dissipationless.

We here illustrate the cusp-core transition as a transformation between two DARKexp halos. We can use DARKexp as a starting point for modeling baryonic effects if they are mostly non-collisional, in which case DARKexp is also a good descriptor of the final state. Note, however, that we do not intend to model the details of the transition in terms of detailed physics (e.g., Oñorbe et al. 2015) such as the mass accretion history or star-formation history of the system, the supernova energy deposition efficiency, or the stellar initial mass function.

Cusps or cores of dark matter halos are governed by the normalized dimensionless depth of the central potential well, to the extent that their potentials are shaped by collective relaxation. How different are halos with different normalized central potentials, apart from their central logarithmic density slopes? We obtain analytical expressions for their total potential energies in Appendix A. We can also express the total potential energy of a halo as

$$W = -\zeta \frac{GM^2}{r_h} \quad (8)$$

with $\zeta \approx 0.4$ (Spitzer 1969) (see Figure 4). Here M is the total mass (which is finite for DARKexp and the γ -models) and r_h is the half-mass radius.

For a γ -model, the halo binding energy relative to an NFW cusp model, i.e., $\gamma_{\text{cusp}} = 1$, is $|\Delta W/2W_{\text{core}}| =$

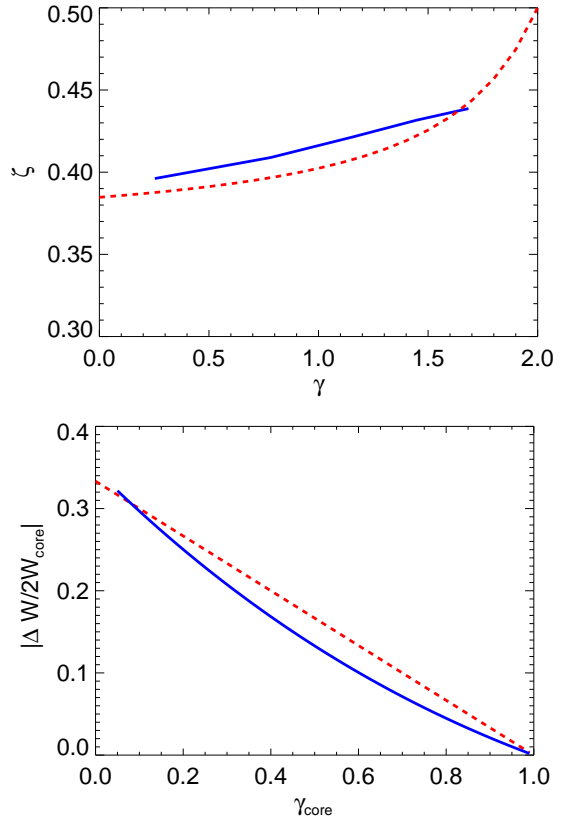


Figure 4. Left: The prefactor ζ in Equation (8) for DARKexp (blue, solid) and the γ -models (red, dashed). Right: Relative energy required to transform an NFW cusp (logarithmic slope -1) into a core with central observed logarithmic slope of γ_{core} . We plot $|\Delta W/2W_{\text{core}}|$ for DARKexp (blue, solid) and the γ -models (red, dashed), given by Equations (A4) and (A6), respectively. In both panels, γ for DARKexp was obtained from Equation (5).

$1/3(1 - \gamma_{\text{core}})$ (Equation A6). This relation is plotted in Figure 4 along with the corresponding relation based on DARKexp. The binding energy of a cored halo ($\gamma_{\text{core}} = 0$) is $\sim 30\%$ less than that of a cuspy halo ($\gamma_{\text{cusp}} = 1$), relative to the binding energy of the cored halo. For $\gamma_{\text{core}} = 0.5$, $\gamma_{\text{cusp}} = 1.5$ the difference is $\sim 25\%$. These differences are significant, i.e., halos do not have universal structures or relative binding energies if they have different central cusp strengths.

For a dwarf galaxy with virial mass $M = 3 \times 10^9 M_{\odot}$, $r_h = 10$ kpc, the total potential energy is $W \approx 3 \times 10^{55}$ erg. The cusp-core transition therefore requires $\sim 10^{55}$ erg or $\sim 10^4$ supernovae (for a supernova energy input of $\sim 10^{51}$ erg) for $\gamma_{\text{core}} = 0$ (higher values of γ_{core} require less energy input). This corresponds to a total stellar mass produced of $\sim 10^6 M_{\odot}$, with an uncertainty of about a factor of 2 depending on the initial mass function. These estimates are consistent with those of Peñarrubia et al. (2012) and Garrison-Kimmel et al. (2013). Because supernovae do not transfer all their kinetic energy into the dark matter, the energy injection is less efficient and more supernovae are needed. On the other hand, the energy input needed is diminished when considering the actual star formation and mass assembly history of dwarf spheroidals (Amorisco et al. 2014; Madau et al. 2014). Finally, observations do not strictly require $\gamma = 0$, further reducing the energy requirements.

As discussed in Section 3.2, dark matter halos of clusters of galaxies also appear to have central logarithmic slopes that are more shallow than -1 (Sand et al. 2004; Zitrin & Broadhurst 2009; Newman et al. 2013b,a). The effect seems to be generic (Newman et al. 2013a), giving central logarithmic slopes in the range 0.2–0.8. While some of this may be due to substructure, line of sight effects, or elongated structures (e.g., due to merging), it does appear that central profiles more shallow than NFW are observed in clusters of galaxies. However, for a massive cluster of galaxies with $M = 1 \times 10^{15} M_{\odot}$ and $r_h = 500$ kpc, the energy input required is $\sim 10^{64}$ erg, corresponding to an unrealistic total stellar mass of $10^{15} M_{\odot}$, if supernovae were to provide the energy input. It is therefore unlikely that supernova feedback is the origin of cores in clusters of galaxies. It is possible that dynamical friction (El-Zant et al. 2001) of infalling satellites or black holes, active galactic nuclei (Martizzi et al. 2012) or cluster mergers (Newman et al. 2013a) (although see Dehnen 2005) may provide the energy injection needed to erase the central cusp. Some clusters may also be born with a shallow potential, although it is noteworthy that a fair fraction of simulated cluster dark halos have central logarithmic slopes steeper than -1 .

5. CONCLUSIONS

It has become standard practice to fit spherically averaged density profiles of dark matter halos, galaxies and clusters with phenomenological models, such as the NFW or its variants, or the Einasto α -model. We suggest that the reason these functions fit well is because they happen to resemble DARKexp, which is a theoretically derived model for collisionless self-gravitating systems, based on statistical mechanical arguments.

Moreover, in this paper we have argued that non-universality of dark-matter halos is a natural expectation of DARKexp. If dark-matter halos would have logarithmic slopes at small radii robustly resolved in simulations equal to -1 , this would require some fine tuning of the model. The expectation of a range of properties appears to be borne out in simulations, and in observations of dwarf galaxies, and clusters of galaxies. In this picture, the range of central logarithmic slopes inferred can be seen as a reflection of a range in their central normalized potentials, or, equivalently, their total normalized binding energies. This insight is useful when quantifying the extent to which halos differ as a result of their formation history and also can be used to analytically relate halos with different cusps to each other, such as required in the cusp-core transition. We do not suggest that the central potential is set up by some external process which then in turn causally sets the density profile. Rather, the central potential and the logarithmic slope of the density profiles are both signatures of an underlying formation process which determines the final equilibrium state. Future data on both dwarfs and clusters will be necessary to more fully examine the applicability of DARKexp to the whole range of systems.

Because DARKexp does not have an analytical density profile, and if using tables of DARKexp $\rho(r)$ is not an option, we have identified phenomenological fitting functions that match DARKexp reasonably well, and have presented relations between DARKexp's ϕ_0 and the best

fitting γ of the γ -model, and α of the Einasto model. The resulting DARKexp (Hjorth & Williams 2010) density profiles are well represented by Dehnen–Tremaine γ -models (Dehnen 1993; Tremaine et al. 1994). The main advantage of these models is that they allow for a range of values of the central cusp logarithmic slope and so can be used to model both the standard NFW-type halos with $d \log \rho(r)/d \log r \approx -1$ as well as more shallow (or steep) halos.

As shown in this paper (Figures 1 and 3) and in other recent work (Gao et al. 2008; Springel et al. 2008; Vera-Ciro et al. 2013; Ludlow et al. 2013), cold dark matter numerical simulations by themselves generate a significant dispersion in α of simulated halos, reflecting different formation, accretion, or tidal stripping histories. DARKexp naturally accounts for such non-universality in profile shapes. In Figure 3 we demonstrate the non-universality of the pure dark matter halos. Both the shallower and the steeper systems are well fit by DARKexp. While we have demonstrated a significant non-universality found in simulations of massive dark-matter halos, with a similar dispersion noticeable in simulations of lower mass halos (e.g., Ludlow et al. 2013), it would be important to quantify the degree of non-universality and range of central potentials realized as a function of halo mass (see also Di Cintio et al. 2014).

In Section 4 we compare the potential energies associated with the core and cusp systems and discuss the required amount of energy and the possible injection mechanisms to bring about the transformation from a steeper pure dark matter system to a shallower observed system. The cusp–core transition cannot be simply modeled as a ‘one-size-fits-all’ transition from an NFW halo (or a DARKexp with $\phi_0 \sim 3 - 4$) to a cored halo (or a DARKexp with $\phi_0 < 2$), because for both dwarf galaxies (Collins et al. 2014) and clusters (Newman et al. 2013a) there is a real dispersion in their observed properties. As highlighted in this paper the same is true for simulated massive dark-matter halos (see Ludlow et al. 2013; Di Cintio et al. 2013, for other mass ranges). When modeling any transition of the central logarithmic slope properties as a result of some energy injection process, it is important to consider the significant dispersion in both the initial dark matter halos and those observed or affected by energy injection processes.

Finally, we note that the ϕ_0 – γ relation (Figure 1) can be directly tested in numerical simulations, e.g., dissipationless collapse or cosmological simulations. Halos with steeper profiles should have deeper central normalized potentials (possibly due to different formation times and accretion histories). For clusters of galaxies the ϕ_0 – γ relation can be probed using gravitational redshift measurements (Wojtak et al. 2011) of the central potential and gravitational lensing measurements of the density profiles (Umetsu et al. 2011; Beraldo e Silva et al. 2013; Umetsu et al. 2015).

We would like to thank Drew Newman for kindly providing us with their galaxy cluster fits and Nicola Amorisco, Arianna Di Cintio, Marceau Limousin, Keiichi Umetsu, and Jesús Zavala for comments. The Dark Cosmology Centre (DARK) is funded by the Danish National Research Foundation. L.L.R.W. would like to thank DARK for their hospitality.

APPENDIX

A. POTENTIAL ENERGY OF CORED AND CUSPY DARKEXP AND γ -MODELS

For DARKexp, $N(\epsilon) = \exp(\phi_0 - \epsilon) - 1$,

$$M(\phi_0) = \int_0^{\phi_0} N(\epsilon) d\epsilon = \exp \phi_0 - (\phi_0 + 1) \quad (\text{A1})$$

and

$$K + 2W = - \int_0^{\phi_0} \epsilon N(\epsilon) d\epsilon, \quad (\text{A2})$$

where K is the total kinetic energy and W is the total potential energy. Using the virial theorem, $W = -2K$,

$$\frac{3}{2}W = -M(\phi_0) + \frac{\phi_0^2}{2}. \quad (\text{A3})$$

Assuming unit-mass DARKexp models, the energy difference between a cusp and a core relative to the current core is

$$\left| \frac{\Delta W}{2W_{\text{core}}} \right| = \frac{1}{2} \left(\frac{2 - \frac{\phi_0^2}{M(\phi_0)} \Big|_{\text{cusp}}}{2 - \frac{\phi_0^2}{M(\phi_0)} \Big|_{\text{core}}} - 1 \right). \quad (\text{A4})$$

For a γ -model normalized to unit mass, $\rho = \frac{3-\gamma}{4\pi} r^{-\gamma} (1+r)^{\gamma-4}$,

$$W = -(10 - 4\gamma)^{-1} \quad (\text{A5})$$

and

$$\left| \frac{\Delta W}{2W_{\text{core}}} \right| = \frac{1}{2} \left(\frac{5 - 2\gamma_{\text{core}}}{5 - 2\gamma_{\text{cusp}}} - 1 \right). \quad (\text{A6})$$

For the unit-mass γ -models, the relation between central potential and inner logarithmic slope is

$$\phi_\gamma = (2 - \gamma)^{-1}. \quad (\text{A7})$$

The relevant radii are also directly related to γ through

$$r_{-2} = 1 - \gamma/2 \quad (\text{A8})$$

and the half-mass radius,

$$r_h = (2^{1/(3-\gamma)} - 1)^{-1} \quad (\text{A9})$$

(Dehnen 1993). Note that $\phi_\gamma r_{-2} = 0.5$ for γ -models; $\phi_0 r_{-2} \approx 0.5$ also holds for a unit mass DARKexp, further demonstrating that the two models are similar.

B. PHENOMENOLOGICAL FITS TO DARKEXP

Figure 5 shows a comparison between DARKexp and Einasto profiles. The correspondence is very good at small radii but poor at large radii. The poorer fit at larger radii is because the Einasto profile does not have a ‘built-in’ outer logarithmic slope of -4 , except for values around the canonical $\alpha = 0.17$. The profiles were matched in density, so the corresponding blue and green curves intersect each other at r_a . The dashed curves in the same plot are the corresponding logarithmic density slopes; here too Einasto models track the respective DARKexp very well, although the blue and green dashed curves do not intersect each other at r_a because the models can be matched either in density, or logarithmic density slope, not both.

The left panel of Figure 6 shows DARKexp of $\phi_0 = 2, 4, 6$ as solid blue curves, and the matched γ -models (Equation 3) as red solid curves. These were matched in density. The γ -models approximate DARKexp very well over nearly 4 decades in radius. The right panel of Figure 6 shows the same DARKexp density profiles with the γ -models that were matched in logarithmic density slope, at r_a . These too provide very good fits to DARKexp.

Figure 7 shows the effect of varying β in the generalized Hernquist model (Equation 2), between 0.5 and 2.0 (here we show model pairs matched only in density, not logarithmic slope). A value of $\beta = 0.7$ appears to provide a slightly better fit than $\beta = 1$ but the improvement is not sufficiently significant to justify the introduction of another parameter. Note, however, that in the inner parts the correspondence with DARKexp is inferior to that of the Einasto profile, despite the fact that the generalized Hernquist model has an extra shape parameter. Overall, γ -models appear to be useful representations of DARKexp.

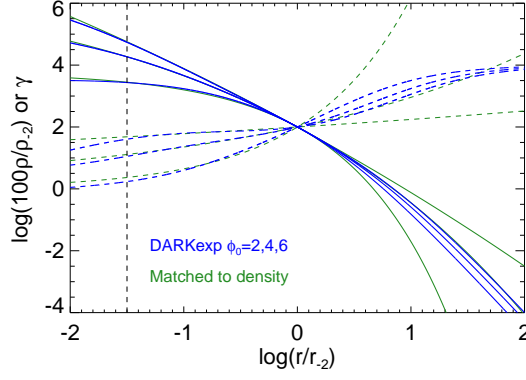


Figure 5. Comparison of DARKexp and Einasto models. DARKexp models with $\phi_0 = 2, 4, 6$ (from bottom to top at small radii) are shown in blue (solid curves: density profile; dashed curves: logarithmic density slope). In green we show α -models matched at $\log(r_a/r_{-2}) = -1.5$ (dashed black lines) in density.

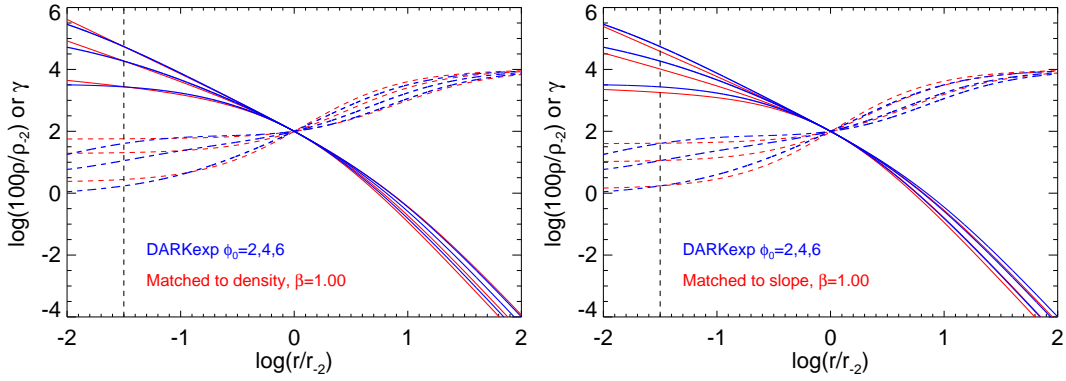


Figure 6. Comparison of DARKexp and γ -models (similar to Figure 2). In red we show γ -models (Hernquist models with $\beta = 1$) matched at $\log(r_a/r_{-2}) = -1.5$ lines in either density (left) or logarithmic slope (right).

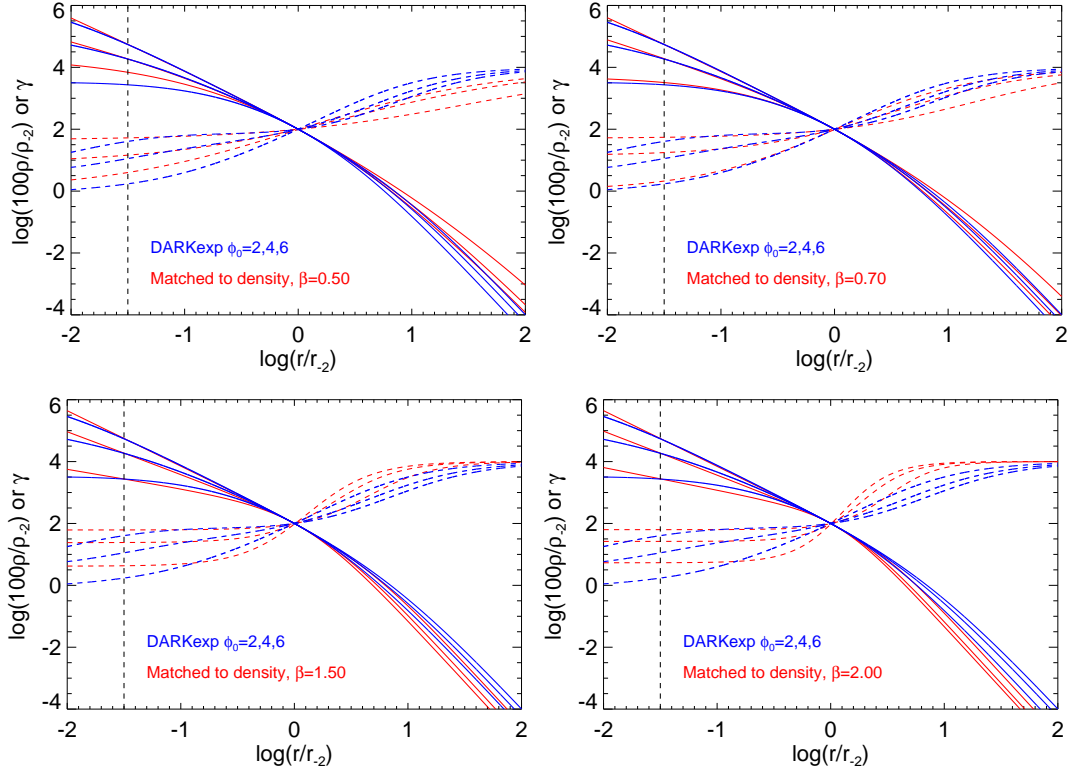


Figure 7. Effects of varying β between 0.5 and 2.0. Matching is done in density at $\log(r/r_{-2}) = -1.5$ like in Figure 6 (left).

REFERENCES

- Adams, J. J., et al. 2014, *ApJ*, 789, 63
 Amorisco, N. C., Agnello, A., & Evans, N. W. 2013, *MNRAS*, 429, L89
 Amorisco, N. C., & Evans, N. W. 2012, *MNRAS*, 419, 184
 Amorisco, N. C., Zavala, J., & de Boer, T. J. L. 2014, *ApJ*, 782, L39
 Beraldo e Silva, L. J., Lima, M., & Sodr e, L. 2013, *MNRAS*, 436, 2616
 Boylan-Kolchin, M., Bullock, J. S., & Kaplinghat, M. 2011, *MNRAS*, 415, L40
 Brook, C. B., Stinson, G., Gibson, B. K., Wadsley, J., & Quinn, T. 2012, *MNRAS*, 424, 1275
 Collins, M. L. M., et al. 2014, *ApJ*, 783, 7
 Dehnen, W. 1993, *MNRAS*, 265, 250
 —. 2005, *MNRAS*, 360, 892
 Di Cintio, A., Brook, C. B., Dutton, A. A., Macci , A. V., Stinson, G. S., & Knebe, A. 2014, *MNRAS*, 441, 2986
 Di Cintio, A., Knebe, A., Libeskind, N. I., Brook, C., Yepes, G., Gottl ber, S., & Hoffman, Y. 2013, *MNRAS*, 431, 1220
 Diemand, J., & Moore, B. 2011, *Advanced Science Letters*, 4, 297
 Diemand, J., Moore, B., & Stadel, J. 2004, *MNRAS*, 353, 624
 —. 2005a, *Nature*, 433, 389
 Diemand, J., Zemp, M., Moore, B., Stadel, J., & Carollo, C. M. 2005b, *MNRAS*, 364, 665
 Einasto, J. 1965, *Trudy Astrofizicheskogo Instituta Alma-Ata*, 5, 87
 El-Zant, A., Shlosman, I., & Hoffman, Y. 2001, *ApJ*, 560, 636
 Flores, R. A., & Primack, J. R. 1994, *ApJ*, 427, L1
 Gao, L., Navarro, J. F., Cole, S., Frenk, C. S., White, S. D. M., Springel, V., Jenkins, A., & Neto, A. F. 2008, *MNRAS*, 387, 536
 Garrison-Kimmel, S., Rocha, M., Boylan-Kolchin, M., Bullock, J. S., & Lally, J. 2013, *MNRAS*, 433, 3539
 Gilmore, G., Wilkinson, M. I., Wyse, R. F. G., Kleyna, J. T., Koch, A., Evans, N. W., & Grebel, E. K. 2007, *ApJ*, 663, 948
 Governato, F., et al. 2012, *MNRAS*, 422, 1231
 Hernquist, L. 1990, *ApJ*, 356, 359
 Hjorth, J., & Madsen, J. 1991, *MNRAS*, 253, 703
 Hjorth, J., & Williams, L. L. R. 2010, *ApJ*, 722, 851
 Jaffe, W. 1987, in *IAU Symposium*, Vol. 127, *Structure and Dynamics of Elliptical Galaxies*, ed. P. T. de Zeeuw, 511
 Jardel, J. R., & Gebhardt, K. 2013, *ApJ*, 775, L30
 Klypin, A., Yepes, G., Gottl ber, S., Prada, F., & Hess, S. 2014, arXiv:1411.4001
 Klypin, A. A., Trujillo-Gomez, S., & Primack, J. 2011, *ApJ*, 740, 102
 Limousin, M., et al. 2008, *A&A*, 489, 23
 Lovell, M. R., Frenk, C. S., Eke, V. R., Jenkins, A., Gao, L., & Theuns, T. 2014, *MNRAS*, 439, 300
 Lovell, M. R., et al. 2012, *MNRAS*, 420, 2318
 Ludlow, A. D., Navarro, J. F., White, S. D. M., Boylan-Kolchin, M., Springel, V., Jenkins, A., & Frenk, C. S. 2011, *MNRAS*, 415, 3895
 Ludlow, A. D., et al. 2013, *MNRAS*, 432, 1103
 Macci , A. V., Paduroiu, S., Anderhalden, D., Schneider, A., & Moore, B. 2012, *MNRAS*, 424, 1105
 —. 2013, *MNRAS*, 428, 3715
 Madau, P., Shen, S., & Governato, F. 2014, *ApJ*, 789, L17
 Martizzi, D., Teyssier, R., Moore, B., & Wenz, T. 2012, *MNRAS*, 422, 3081
 Merritt, D., Graham, A. W., Moore, B., Diemand, J., & Terzi , B. 2006, *AJ*, 132, 2685
 Moore, B. 1994, *Nature*, 370, 629
 Navarro, J. F., Eke, V. R., & Frenk, C. S. 1996, *MNRAS*, 283, L72
 Navarro, J. F., Frenk, C. S., & White, S. D. M. 1997, *ApJ*, 490, 493
 Navarro, J. F., et al. 2004, *MNRAS*, 349, 1039
 —. 2010, *MNRAS*, 402, 21
 Neto, A. F., et al. 2007, *MNRAS*, 381, 1450
 Newman, A. B., Treu, T., Ellis, R. S., & Sand, D. J. 2013a, *ApJ*, 765, 25
 Newman, A. B., Treu, T., Ellis, R. S., Sand, D. J., Nipoti, C., Richard, J., & Jullo, E. 2013b, *ApJ*, 765, 24
 O norbe, J., Boylan-Kolchin, M., Bullock, J. S., Hopkins, P. F., Ker s, D., Faucher-Gigu re, C.-A., Quataert, E., & Murray, N. 2015, arXiv:1502.02036
 Pe arrubia, J., Pontzen, A., Walker, M. G., & Kozlov, S. E. 2012, *ApJ*, 759, L42
 Pontzen, A., & Governato, F. 2012, *MNRAS*, 421, 3464
 —. 2014, *Nature*, 506, 171
 Power, C., Navarro, J. F., Jenkins, A., Frenk, C. S., White, S. D. M., Springel, V., Stadel, J., & Quinn, T. 2003, *MNRAS*, 338, 14
 Riebe, K., et al. 2013, *Astronomische Nachrichten*, 334, 691
 Rocha, M., Peter, A. H. G., Bullock, J. S., Kaplinghat, M., Garrison-Kimmel, S., O norbe, J., & Moustakas, L. A. 2013, *MNRAS*, 430, 81
 Sand, D. J., Treu, T., Smith, G. P., & Ellis, R. S. 2004, *ApJ*, 604, 88
 Shao, S., Gao, L., Theuns, T., & Frenk, C. S. 2013, *MNRAS*, 430, 2346
 Shen, S., Madau, P., Conroy, C., Governato, F., & Mayer, L. 2014, *ApJ*, 792, 99
 Spitzer, Jr., L. 1969, *ApJ*, 158, L139
 Springel, V., et al. 2008, *MNRAS*, 391, 1685
 Strigari, L. E., Bullock, J. S., Kaplinghat, M., Kravtsov, A. V., Gnedin, O. Y., Abazajian, K., & Klypin, A. A. 2006, *ApJ*, 652, 306
 Strigari, L. E., Frenk, C. S., & White, S. D. M. 2014, arXiv:1406.6079
 Tasitsiomi, A., Kravtsov, A. V., Gottl ber, S., & Klypin, A. A. 2004, *ApJ*, 607, 125
 Tremaine, S., Richstone, D. O., Byun, Y.-I., Dressler, A., Faber, S. M., Grillmair, C., Kormendy, J., & Lauer, T. R. 1994, *AJ*, 107, 634
 Umetsu, K., Broadhurst, T., Zitrin, A., Medezinski, E., Coe, D., & Postman, M. 2011, *ApJ*, 738, 41
 Umetsu, K., Zitrin, A., Gruen, D., Merten, J., Donahue, M., & Postman, M. 2015, arXiv:1507.04385
 Vera-Ciro, C. A., Helmi, A., Starkenburg, E., & Breddels, M. A. 2013, *MNRAS*, 428, 1696
 Vogelsberger, M., Zavala, J., & Loeb, A. 2012, *MNRAS*, 423, 3740
 Vogelsberger, M., Zavala, J., Simpson, C., & Jenkins, A. 2014, *MNRAS*, 444, 3684
 Walker, M. G., Mateo, M., Olszewski, E. W., Pe arrubia, J., Wyn Evans, N., & Gilmore, G. 2009, *ApJ*, 704, 1274
 Walker, M. G., & Pe arrubia, J. 2011, *ApJ*, 742, 20
 Weinberg, D. H., Bullock, J. S., Governato, F., Kuzio de Naray, R., & Peter, A. H. G. 2013, arXiv:1306.0913
 Williams, L. L. R., Barnes, E. I., & Hjorth, J. 2012, *MNRAS*, 423, 3589
 Williams, L. L. R., & Hjorth, J. 2010, *ApJ*, 722, 856
 Williams, L. L. R., Hjorth, J., & Wojtak, R. 2010, *ApJ*, 725, 282
 —. 2014, *ApJ*, 783, 13
 Wojtak, R., Hansen, S. H., & Hjorth, J. 2011, *Nature*, 477, 567
 Zavala, J., Vogelsberger, M., & Walker, M. G. 2013, *MNRAS*, 431, L20
 Zitrin, A., & Broadhurst, T. 2009, *ApJ*, 703, L132
 Zolotov, A., et al. 2012, *ApJ*, 761, 71